Title

Glycan Sulfation Modulates Dendritic Cell Biology and Tumor Growth.

Journal

Neoplasia (New York, N.Y.), 18(5)

ISSN

1522-8002

Authors

El Ghazal, Roland

Yin, Xin

Johns, Scott C

et al.

Publication Date

2016-05-01

DOI

10.1016/j.neo.2016.04.004

Peer reviewed

NEOPLASIA
www.neoplasia.com

Volume 18 Number 5 May 2016 pp. 294–306 294

Glycan Sulfation Modulates Dendritic Cell Biology and Tumor Growth[1]

Roland El Ghazal[*,†], Xin Yin[*,†,‡], Scott C. Johns[*,†], Lee Swanson[§], Monica Macal[¶], Pradipta Ghosh[§], Elina I. Zuniga[¶] and Mark M. Fuster[*,†,#]

*VA San Diego Healthcare System, Medical and Research Sections, La Jolla, CA 92161; [†]Department of Medicine, Division of Pulmonary and Critical Care, University of California San Diego, La Jolla, CA 92037; [‡]Jiangsu Key Laboratory of Marine Pharmaceutical Compound Screening, School of Pharmacy, Huaihai Institute of Technology, Lianyungang, China; [§]Division of Gastroenterology, University of California San Diego, La Jolla, CA 92093; [¶]Division of Biological Sciences, University of California San Diego, La Jolla, CA 92093; [#]Glycobiology Research and Training Center, University of California San Diego, La Jolla, CA 92093

Abstract

In cancer, proteoglycans have been found to play roles in facilitating the actions of growth factors, and effecting matrix invasion and remodeling. However, little is known regarding the genetic and functional importance of glycan chains displayed by proteoglycans on dendritic cells (DCs) in cancer immunity. In lung carcinoma, among other solid tumors, tumor-associated DCs play largely subversive/suppressive roles, promoting tumor growth and progression. Herein, we show that targeting of DC glycan sulfation through mutation in the heparan sulfate biosynthetic enzyme N-deacetylase/N-sulfotransferase-1 (Ndst1) in mice increased DC maturation and inhibited trafficking of DCs to draining lymph nodes. Lymphatic-driven DC migration and chemokine (CCL21)-dependent activation of a major signaling pathway required for DC migration (as measured by phospho-Akt) were sensitive to *Ndst1* mutation in DCs. Lewis lung carcinoma tumors in mice deficient in *Ndst1* were reduced in size. Purified CD11c + cells from the tumors, which contain the tumor-infiltrating DC population, showed a similar phenotype in mutant cells. These features were replicated in mice deficient in syndecan-4, the major heparan sulfate proteoglycan expressed on the DC surface: Tumors were growth-impaired in syndecan-4–deficient mice and were characterized by increased infiltration by mature DCs. Tumors on the mutant background also showed greater infiltration by NK cells and NKT cells. These findings indicate the genetic importance of DC heparan sulfate proteoglycans in tumor growth and may guide therapeutic development of novel strategies to target syndecan-4 and heparan sulfate in cancer.

Neoplasia (2016) 18, 294–306

Address all correspondence to: Mark M. Fuster, MD, VA San Diego Healthcare System and UCSD Department of Medicine, Division of Pulmonary & Critical Care, 3350 La Jolla Village Drive, San Diego, CA 92161-111J.
E-mail: mfuster@ucsd.edu

[1]Funding Support: We acknowledge funding from National Insitutes of Health/National Heart, Lung, and Blood Institute (R01-HL107652 to M. M. F.) as well as the Merit Review Program (VA-Merit I01BX000987-01 to M. M. F.) and from National Insitutes of Health/National Heart, Lung, and Blood Institute (T32-HL098062 to X. Y. and R. E.), National Institute of Allergy and Infectious Diseases (R01-AI081923 to E.I.Z.), and support from the Veterans Medical Research Foundation (M. M. F.). E.I.Z. is also a Leukemia and Lymphoma Society Scholar. L.S was supported by a pre-doctoral training award from the NIH (T32DK0070202).
Received 24 December 2015; Revised 13 April 2016; Accepted 14 April 2016

1476-5586
http://dx.doi.org/10.1016/j.neo.2016.04.004

Introduction

Dendritic cells (DCs) are professional antigen-presenting cells that play a pivotal role in the regulation of innate and adaptive immunity. They can either prime the adaptive immune system to eliminate unwanted antigens or allow tolerance to antigens recognized as self [1]. These strikingly polarized functions of DCs seem to be regulated in part via by-products of microbial pathogens (LPS, peptidoglycans, CpG motifs, viral nucleic acids) and microenvironment-dependent cues such as immunostimulatory cytokines (TNFα, IL-1) or immune-inhibitory cytokines (TGF_β, IL-10, PGE_2) [2,3]. In cancer, the latter often predominate and promote a tolerogenic immature DC phenotype. The induction of cellular immunity against tumors requires DCs to transform from a chemokine-responsive, hypermotile, immature state to a more hypomotile, mature antigen-presenting state. A failure to do so may promote immune tolerance. We investigated herein how endogenous glycans on DCs might mediate this functional state and how targeting their fine structure might affect tumor growth and immunity.

Heparan sulfate (HS) is a glycosaminoglycan covalently linked to a distinct family of proteoglycan core proteins on the cell surface or in extracellular matrix. HS proteoglycans (HSPGs) play particularly important roles in mediating chemokine and growth factor binding and receptor signaling at the cell surface by virtue of unique sulfate-modified domains along the HS carbohydrate chains [4]. The latter are known to mediate interactions with basic amino acid regions of ligands that bind to the relevant proteins. Proteoglycans are ubiquitously present on cell surfaces [5], basement membranes [6], and connective tissue [7] and are released during inflammatory [8] and immune processes [9]. Moreover, soluble HS can act as a sensor of tissue injury and endogenous damage-associated molecular pattern molecules [10], with the ability to directly interact with TLR-4 [11].

Early reports suggested a role for soluble HS and heparin (a highly sulfated mast cell–derived form of HS) in lymphocyte activation [12,13]. Soluble HS induces phenotypic maturation of murine immature DCs with upregulation of I-A, CD40, ICAM-1, CD80, and CD86 [14]. It also stimulates murine alloreactive T cells *in vitro* through DC activation, leading to an increase in maturation markers CD40 and CD80 and increased proinflammatory cytokines IL-6 and IL-12 [15]. This phenomenon was also noted in other antigen-presenting cells, including macrophages and B cells [16]. In addition, heparin induces differentiation of human $CD1a^+$ DCs from monocytes with increased expression of maturation markers CD40 and CD80, including greater potency in priming allogenic and autologous $CD4^+$ T-cell proliferation [17]. Heparin added to monocyte-conditioned medium also induces expression of DC maturation marker CD83 in human monocyte-derived DCs, with a greater response to the mixed leukocyte reaction [18].

Although DC maturation may be critically modulated by glycans, another key consideration is lymphatic cell traffic. The fine structure of HS may facilitate the actions of major lymphatic-microenvironment chemokines, such as CCL21 required for chemotaxis of classic DCs toward the lymph node from the periphery. For CCL21 in particular, DC responses depend on expression of the cognate chemokine receptor CCR7 on the DC surface. Although basic amino acids of CCL21 bind strongly to sulfated domains of HS (with as high as 1.0 M NaCl required to elute CCL21 from a heparin column), it is unknown whether HS produced on DCs may serve as a co-receptor to facilitate CCL21 binding. This might involve binding to either HS or CCR7 as facilitated by HS (possibly simultaneously) on the DC cell surface. Heparan sulfate also appears to play a key role in lymphocyte and DC chemotaxis through interactions with adhesion molecules involved in cell trafficking (e.g., β1 integrins) and binding to other chemokines. The latter may facilitate formation of chemokine-receptor ternary complexes [19,20] that involve G-protein coupled receptors (GPCRs). Heparan sulfate has been shown to participate in transcytosis as well as gradient formation by chemokines that also promote lymphocyte and neutrophil migration across blood vasculature [21–23]. Given these cell trafficking considerations, it is important to consider the importance of DC-endogenous HS as well as HS proteoglycans in DC trafficking.

Three known subfamilies of HSPGs, which include membrane-spanning HSPGs (e.g., syndecans), glycophosphatidyl inositol–linked HSPGs (e.g., glypicans), and secreted HSPGs (e.g., perlecan, agrin, and collagen XVIII) [4], may play particularly important roles in displaying HS glycosaminoglycan chains on the cell surface of DCs. For example, the HSPG syndecan-4 on DCs may serve as an integrin-associated co-receptor mediating DC motility [24] as well as interactions with the extracellular matrix. It appears to be upregulated by DC maturation and may somehow facilitate coupling of DC activation to DC motility [25]. On the other hand, syndecan-4 may be inactivated in human monocyte-derived DCs, partly through the action of lysophosphatidylcholine, which is generated during apoptosis and inhibits DC motility [26].

In this report, we examined the genetic importance of HS sulfation on DCs for the promotion of chemokine-dependent motility in the lymphatic microenvironment, a process that appears to promote pathologic progression in cancer. We also probed the functional effects of such genetic targeting on DC maturation and also carried this out with an eye toward cancer biology. We questioned whether the DC phenotype as a result of such genetic targeting might extend to tumor-derived DCs and whether this might affect DC-mediated immunity in carcinoma. We demonstrate herein that reducing the sulfation or abundance of HS on the DC surface through novel genetic methods results in unique features of DC hypomotility and hypermaturation, with blunting of nonspecific DC antigen sensing. Extending this genetic targeting to tumors resulted in reduced tumor growth with preservation of these DC functional features and an antitumor immunophenotype.

Material and Methods

Cell Cultures

C57Bl/6 mouse primary lymphatic endothelial cells (mLEC, CellBiologics, C57-6092) were cultured with complete mouse endothelial cell culture medium using a kit (CellBiologics, M1168). Lewis lung carcinoma (LLC) cells (LL/2, ATCC, CRL-1642) were cultured in Dulbecco's modified Eagle's medium (DMEM) (Corning, 10-013) supplemented with 10% heat-inactivated fetal bovine serum (Atlanta Biologicals, S11150H). Bone marrow–derived DCs (BMDCs) were obtained from mice as previously described [27] with some modifications. Briefly, mice were sacrificed at age 2 to 6 months, with bone marrow cells flushed from femurs and tibias using a syringe containing RPMI-1640 with a 25-g needle, and addition to a 100-mm petri dish (~2 million cells per dish) with 10 ml of RPMI-1640 (Corning, 10-040) that was supplemented with the following: penicillin-streptomycin (100 U/ml and 100 μg/ml, respectively, Sigma-Aldrich, P4333), L-glutamine (2 mM, Corning, 25-005), beta-mercaptoethanol (55 μM, Gibco, 21985), 10%

heat-inactivated fetal bovine serum, 1 mM nonessential amino acids (Invitrogen, 11140),10 mM HEPES (Affymetrix, 16924), and 20 ng/ml of GM-CSF (Peprotech, 315-03). Fresh medium (10 ml) was added to the cells on days 3,6, and 8. Day 8 or 9 mature BMDCs were obtained with or without the addition of 10 ng/ml of LPS from *Escherichia coli* 055:B5 (Sigma-Aldrich, L6529). Flow cytometry using anti-CD11c demonstrated 78% and 92% purity of DCs at day 8 and 9, respectively.

Genetic Mouse Models

In addition to using wild-type C57Bl/6 mice to generate tumors for tumor-infiltrating dendritic cells (TIDCs) and BMDCs from normal mice, cells were also obtained from genetic mouse models. In one model, *Cre*-dependant N-deacetylase/N-sulfotransferase-1 (*Ndst1*) deficiency is achieved in the myeloid lineage. Specifically, *Cre*-mediated deletion of a loxP-flanked segment of the *Ndst1* Exon-2 coding region is achieved under the control of the Lysozyme-2 promoter/enhancer, expressed at high frequency in the myeloid lineage. Such $Ndst1^{fff}$ $LysMCre^{+}$ animals were extensively backcrossed onto the C57Bl/6 background and were noted to have ~90% reduction in *Ndst1* mRNA expression by quantitative polymerase chain reaction (qPCR) (Supplemental Figure S1) in isolated BMDCs. Another model involved syndecan-4 knockout ($Sdc4^{-/-}$) mice, which were originally obtained as a kind gift from Dr. Paul Goetinck, and bear a constitutional deficiency in the HS proteoglycan syndecan-4. For some studies, these were used to generate BMDCs. The BMDCs isolated from $Sdc4^{-/-}$ mice were confirmed to have >99.8% reduction in *Sdc4* mRNA by qPCR compared with cells derived from wild-type mice. Otherwise, all animal studies, including tumor-based *in vivo* models, were approved by the local institutional animal care and use committee.

Tumor Model and Extraction of TIDCs from $Ndst1^{fff}$ $LysMCre$ Mutants

The subcutaneous LLC tumor model was employed by injecting 2.5×10^5 LL/2 LLC cells in 50 µl DPBS subcutaneously using a 25-g needle in the mouse left lower abdominal wall and harvesting tumors at day 20. Mice were euthanized using carbon dioxide according to current American Veterinary Medical Association guidelines. Tumors were extracted in a sterile fashion, weighed, and minced with scissors and digested for 1 hour in a digestion buffer solution containing DMEM, 0.2% collagenase from *Clostridium histolyticum* (Sigma-Aldrich, C2799), and 15 µg/ml DNAse I (Sigma-Aldrich, D4513). Single-cell suspensions were obtained by filtering through a 40-µm cell strainer (Fisherbrand, 22363547). Magnetic separation of DCs ($CD11c^{+}$ cells) was performed according to Miltenyi Biotec manufacturer instructions. Briefly, cells were magnetically labeled with CD11c MicroBeads (120-000-322), loaded onto a MACS MS column (130-042-20), and placed in the magnetic field of a magnetic separator (MiniMACS 130-042-102). The unlabeled $CD11c^{-}$ cells were depleted by running a MACS buffer solution (DPBS, 0.5% BSA [Gemini Bio-Products 700-100P], and 2 mM EDTA [Sigma-Aldrich, E5134]) through the column. Finally, the MACS MS column was removed from the magnetic field and flushed out using a MACS buffer solution and a plunger to collect the magnetically labeled $CD11c^{+}$ cells.

General DC Flow Cytomety Phenotyping

Most analyses of BMDCs or TIDCs were carried out using flow cytometry with antibodies agains: MHCII-APC-Cy7 (BioLegend 1/100), CD86-PE (eBioscience 1/200), CD11c-FITC (TONBO Biosciences at 1/100), and CCR7-PE (eBioscience, 1/100). Harvested cells were incubated with CD16/32 FC block in FACS buffer (1 × PBS + 1% BSA), with primary antibodies added according to manufacturer recommendations for 30 minutes at 4°C. Cells were washed with ice-cold FACS buffer × 2 and analyzed using BD LSR II. Data were analyzed using FlowJo (V X.0.7).

Transwell Migration Assays

DC motility towards lymphatic endothelial monolayers was assessed using Transwell inserts (5.0 µm in pore size, Corning, 3421). At the bottom of the Transwell, a primary lymphatic endothelial cell monolayer was allowed to grow until cells were ~70% to 90% confluent, with the medium then changed to RPMI-1640. Alternatively, 100 ng/ml of the chemokines mCCL19 (MIP-3β, PeproTech, 250-27B) or mCCL21 (PeproTech, 250-13) was added to the medium (RPMI-1640) at the bottom of the Transwell instead of the lymphatic monolayer. A total of 2.5×10^5 Calcein AM-labeled DCs (following the manufacturer instructions; Invitrogen) were placed on top of the insert in RPMI-1640 and allowed to migrate for 3 hours at a 37°C in a 5% CO_2 incubator. Suspended and adherent cells were collected from the bottom (using Accutase according to manufacturer, Innovative Cell Technologies) and counted using a BD LSR-II flow cytometer. Assays were set up in triplicate. Results were expressed as % migration and, in some cases, as relative migration compared with a negative control.

In Vivo Migration Assay

Calcein-AM labeled BMDCs were washed twice with DPBS (Corning, 21-031), and 2×10^6 cells were injected in 50 µl DPBS into the footpad of C57Bl/6 mice. Corresponding unilateral popliteal lymph nodes were extracted 40 hours later, minced, and digested in 2 ml of digestion buffer solution containing DMEM, collagenase, and DNAse I. Cell numbers were counted using a BD LSR-II Flow Cytometer.

Western Blotting and DC Signaling

Serum-starved BMDCs were stimulated with recombinant mouse CCL21 (100 ng/ml). Lysed cells were frozen in lysis buffer (20 mM HEPES, pH 7.2, 5 mM Mg acetate, 125 mM K acetate, 0.4% Triton X-100, 1 mM DTT, supplemented with sodium orthovanadate [500 µM], phosphatase [Sigma-Aldrich], and protease [Roche] inhibitor cocktails) [28]. Thawed samples were separated on 4% to 15% gradient gels with rabbit-polyclonal antibodies against phospho-(Ser^{473})Akt (1:1000; Cell Signaling) and total-Akt, followed by IRdye-conjugated anti-rabbit antibody (LI-COR). Bands were normalized to the ratio of phospho-/total Akt for baseline-starved cells on an Odyssey/LI-COR infrared system. Replicate assays on independent cell populations were tested to obtain robust data for mean ± SD for Western signal in mutant versus wild-type cells.

Tumor Growth Studies and Tumor Immunophenotyping in Syndecan-4 Mutant Mice

LLC whole-tumor cell digests were thawed from liquid-nitrogen storage, diluted in 1 × PBS, centrifuged, and washed two more times in 1 × PBS to remove freezing media. (Digests were derived from LLC tumors originally established in gene-targeted mice through the subcutaneous injection of 2.5×10^5 LLC cells into the lower abdominal wall and harvesting at 14 days postinjection.) Cells were

counted with trypan blue to account for cell death and incubated with Viability Ghost Dye Violet 510 for 15 minutes at 4°C. Cells were washed and incubated with CD16/32 FC block in FACS buffer (1 × PBS + 1% FBS) for 10 minutes at room temperature. Cells were washed in FACS buffer and incubated with the following antibodies purchased from BD Biosciences, Biolegend, or E-Bioscience (San Diego, CA) for 20 minutes at 4°C: anti-F4/80 Alexa 488, anti-Nk1.1 PE-Texas Red, anti-Thy1.2 Percp-Cy5.5, anti-CD19 Percp-Cy5.5, anti-CD11b Pe Cy7, anti-CD11c Alexa 647, anti-MHC II efluor 450, and anti-CD86 Brilliant Violet 650. Cells were acquired with an LSRII flow cytometer (BD Bioscience), and data were analyzed with FlowJo software (Tree Star, Inc.). A baseline study to examine the effects of muation on continous tumor growth during the early growth period was carried out independently. Tumors were established by injection of 5×10^5 LLC cells into the lower abdominal wall and measuring tumors at regular intervals in real time by caliper (using tumor volume = $[\text{width}]^2 \times$ length/2 to estimate volume).

Endocytosis Assay

BMDCs or TIDCs were incubated at 37°C and 4°C × 1 hour with fluorochrome-conjugated ovalbumin (AF-647 OVA 0.1 mg/ml, Invitrogen, O34784) in FACS buffer. Uptake was stopped by addition of ice-cold FACS buffer and washing three times. Antigen uptake was calculated as follows: (median fluorescence intensity [MFI] of OVA at 37°C minus MFI of OVA at 4°C [nonspecific surface binding]) divided by MFI of OVA from unstained negative control cells

Real-Time Quantitative PCR (RT-qPCR)

Total RNA was extracted from cells using RNAqueous 4-PCR kit (Ambion) and reverse transcribed into cDNA with SuperScript III kit (Invitrogen) according to the manufacturer's instructions. Real-time PCR was performed with iQ Sybr Green Supermix Kit (BioRad) using 100 ng of cDNA. The primer sequences (5′ to 3′) used for real-time PCR were as follows:

Glypican 1 (forward 5′-GCAGGGCCTTCAAGTTTATG-3′; reverse 5′-TGAGCGTAGTATGGCTGTGC-3′),

Glypican 2 (forward 5′-TTTCCTTTGAACTGGCTGCT-3′; reverse 5′-GAGCCACTCTGAAGCCAATC-3′),

Glypican 3 (forward 5′-TTGTTGTTCGCCATGCCAAG-3′; reverse 5′-TTCAGGTCACGTCTTGCTCC-3′),

Glypican 4 (forward 5′-CTACCAACTCCAACTCCCCG-3′; reverse 5′-TTTTCGACTTGAGCTCCGCA-3′),

Glypican 5 (forward 5′-ATCTGGGCATTGAGGTCATC-3′; reverse 5′-CCGGATATAAGCATGCCAGT-3′),

Glypican 6 (forward 5′-TGGCTCCACACATGAGGTTC-3′; reverse 5′-CGCCTCTTGATTCCTTGGGT-3′),

Ndst1 (forward 5′-GGACATCTGGTCTAAG-3′; reverse 5′-GATGCCTTTGTGATAG-3′),

Ndst2 (forward 5′-TGGTCCAAGGAGAAAACCTG-3′; reverse 5′-GGTACGACCTCCGAGTCAAA-3′),

Ndst3 (forward 5′-CCACTGCCTTGTGTC-3′; reverse 5′-GGAGTACGCTCGGTC-3′),

Ndst4 (forward 5′-CTAACTACTTCCACTC-3′; reverse 5′-ATGTGCACTGCATACC-3′),

Sdc1 (forward 5′-GGAGCAGGACTTCACCTTTG-3′; reverse 5′-TACAGCATGAAACCCACCAG-3′),

Sdc2 (forward 5′-GCTGCTCCAAAAGTGGAAAC-3′; reverse 5′-CAGCAATGACAGCTGCTAGG-3′),

Sdc3 (forward 5′-GAGCCTGACATCCCTGAGAG-3′; reverse 5′-CCCACAGCTACCACCTCATT-3′),

Sdc4 (forward 5′-GAGCCCTACCAGACGATGAG-3′; reverse 5′-CAGTGCTGGACATTGACACC-3′),

Cd44v3 (forward 5′-CTGGGAGCCAAATGAAGAAA-3′; reverse 5′-AGCACTTCCGGATTTGAATG-3′)

The PCR cycle conditions were 95°C for 3 minutes followed by 40 cycles of 95°C for 15 seconds, 59°C for 45 seconds, and 72°C for 45 seconds. Relative expression of the target gene was normalized against the expression level of GAPDH using the $2^{-\Delta\Delta Ct}$ method and expressed as target sample mRNA copies per 10^5 copies of GAPDH [29]

Statistics

For some studies involving comparisons of mean values (± SD), means normalized to the wild-type value were compared using the Student's two-tailed *t* test for analysis. Examples include comparison of a mean in a continuous quantity (e.g., tumor volume) in wild-type mice to that of mutant mice or comparing mean Western signals (e.g., poststimulation phospho-/total signal for a given kinase normalized to prestimulation baseline) in mutant versus wild-type cells. Normalization of the mutant value to that of wild-type was used as convention in some cases. For comparisons of some data (e.g., among genotypes) that did not fit a normal distribution, the Wilcoxon signed rank test was used. In some cases, including some determinations in which a ratio varies significantly from 1.0, the Wilcoxon signed rank test was used for statistical analysis with a theoretical median of 1.0. (An example is the ratio of mutant versus wild-type DCs trafficking to the lymph node.) Alternatively, when examining the mean percentage increase or decrease in a value in one group compared with that of another, a theoretical median of 0 was used. An example of the latter is reporting the degree to which mutant DCs are more mature than wild-type DCs (among multiple experiments) or the degree to which ovalbumin uptake is decreased in mutant DCs relative to that of wild-type DCs. Graph Pad PRISM was used for statistical analyses.

Results

Chemokine-Driven DC Migration and HS Chain Sulfation In Vitro and In Vivo

To examine the effect of altering DC-specific HS on DC migration, we first employed modified Transwell assays with the lower-well driving force consisting of primary mLEC monolayers. Migration of DCs in this system depends on lymphatic-secreted chemokines such as the major lymphatic DC-driving chemokine CCL21, known to bind in gradients to matrix- and cell surface–associated HS [30,31]. In the assay, mouse BMDCs harboring a myeloid-targeted mutation in *Ndst1* (*Ndst1*$^{f/f}$ LysM*Cre*$^{+}$), a major enzyme involved in sulfate modification of nascent HS chains [32], showed reduced migration toward mouse lymphatic endothelium (Figure 1*A*). Migration of DCs in the transwell system was confirmed to be sensitive to blockade of CCR7 in separate experiments (not shown). Cultured BMDCs isolated from *Ndst1*$^{f/f}$ LysM*Cre*$^{+}$ mutant mice demonstrated typically anywhere from 70% to 92% inhibition in the expression of *Ndst1*, the dominant Ndst isoenzyme expressed in BMDCs (Supplemental Figure S1). In additional chemokine-driven migration studies, *Ndst1*$^{f/f}$ LysM*Cre*$^{+}$ mutant BMDCs demonstrated reduced migration toward the major heparin-binding CCR7 ligand CCL21 and, interestingly, also showed altered

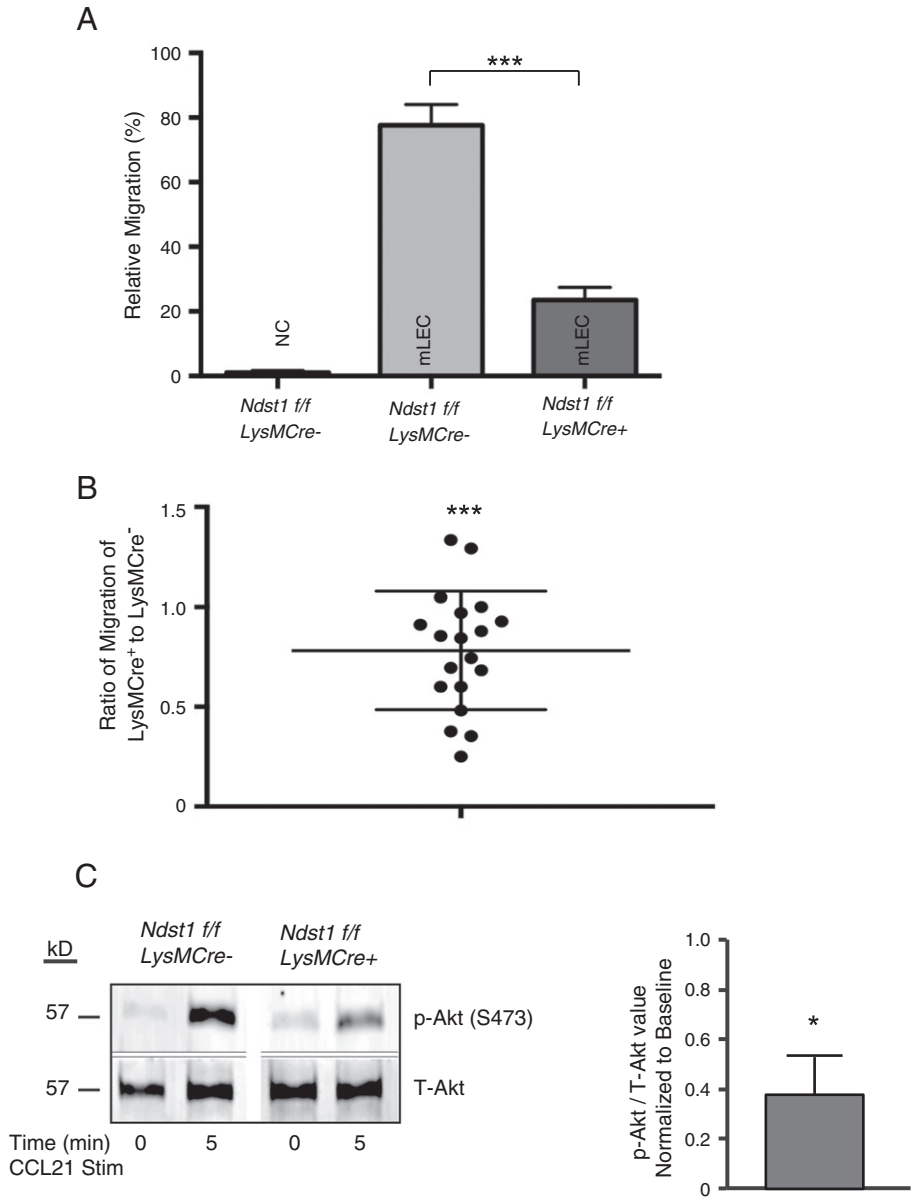

Figure 1. Migration of BMDCs is sensitive to the fine structure of DC HS. (A) A modified Transwell system was employed to examine migration of unstimulated BMDCs with a genetic reduction in HS-chain sulfation (*Ndst1f/f LysMCre* + mutation) toward mouse lymphatic endothelial cell monolayers, with comparison to that of wild-type (*Ndst1f/f LysMCre* −) control cells. Figure is representative of three independent experiments. Two-tailed unpaired *t* test was used for statistical analysis (NC = negative control, wherein lower well contains no lymphatic endothelial cells; ***$P < .001$). (B) BMDCs with genetic *Ndst1* deficiency demonstrate impaired *in vivo* migration toward draining lymph nodes: Relative *in vivo* migration of unstimulated BMDCs with and without altered sulfation of HS toward the popliteal lymph node (following injection at the foot pad) was examined in C57/Bl6 mice. Each dot on the graph represents the ratio of the quantity of right-foot injected *Ndst1f/f LysMCre* + mutant DCs that migrated to the right popliteal lymph node to that of *Cre* − control DCs migrating simultaneously on the left side in a single mouse. Scatter plot is a summary of $N = 19$ mice. Wilcoxon signed rank test was used for statistical analysis with a theoretical median of 1.0; mean = 0.78 ± 0.29 (***$P < .001$). (C) Phosphorylation of Akt in response to stimulation of serum-starved BMDCs with CCL21 was examined at baseline and following 5-minute stimulation in wild-type versus *Ndst1*-deficient BMDCs. Data are normalized to baseline ratio of phospho/total Akt and plotted at lower right. Graph was generated with data from three independent experiments (*$P < .01$ for reduction in mean signal [phospho-Akt/total-Akt value] normalized to baseline in mutant cells as compared with wild-type controls).

migration toward the non–heparin-binding CCR7 ligand, CCL19 (Supplemental Figure S2). Stimulation of cells with LPS prior to migration was associated with more dramatic effects.

In the lymphatic microenvironment of the footpad, nonstimulated *Ndst1*$^{f/f}$LysM*Cre*$^{+}$ BMDCs were impaired in their ability to traffic to the draining popliteal LN as compared with *Cre*$^{-}$ wild-type control cells (Figure 1*B*). This suggests that presence of the mutation in HS N-sulfation is sufficient to inhibit DC lymph node trafficking *in vivo*. Given the above findings, we examined how Ndst1 deficiency in cultured BMDCs might affect CCL21-dependent activation of

migration signaling, which is known to depend on phosphorylation of Akt [33,34]. In Western assays, phospho-Akt was significantly reduced in mutant BMDCs in the early period following CCL21 stimulation (see data for cells at baseline versus 5-minute CCL21; Figure 1*C*). This indicates the importance of appropriately sulfated DC cell-surface HS in GPCR-dependent migration signaling. Representative blot and graph showing densitometry/quantification for an extended (30 minutes) period are shown in Supplemental Figure S3.

Phenotype of DCs with Reduced HS Chain Sulfation

The migration of DCs typically is associated with the maturation state of the cells. As *Ndst1* mutation affects migration (Figure 1), we investigated how *Ndst1* mutation affects the maturation of *ex vivo* cultured BMDCs derived from mutant versus wild-type mice, as assessed using common flow cytometry markers of DC maturation, CD86 and MHC-II. Interestingly, the CD11c$^+$ subset of non-stimulated BMDCs isolated from *Ndst1*$^{f/f}$ *LysMCre*$^+$ mutants showed consistently a greater proportion of mature (MHC-II$^+$ CD86$^+$) cells, along with greater expression of the major lymphatic chemokine receptor CCR7, as compared with BMDCs derived from *Ndst1*$^{f/f}$ *LysMCre*$^-$ littermates (Figure 2*A*). Nearly all (>95%) of the CD11c+ BMDC subset that was MHC-II$^+$ CD86$^+$ also coexpressed CCR7. In BMDCs stimulated with LPS (which is known to augment DC maturation), mutant cells still demonstrated significantly greater maturation than that of wild-type BMDCs, albeit to a lesser extent (Figure 2*B*). The relative increase in mature MHC-II$^+$ CD86$^+$ BMDCs from *Ndst1*$^{f/f}$ *LysMCre*$^+$ mutants compared with *Ndst1*$^{f/f}$ *LysMCre*$^-$ controls without and with LPS stimulation was 29.5 ± 10.1% and 3.5 ± 2.2%, respectively (Figure 2*B*).

Maturation of DCs from Sdc4$^{-/-}$ *Mice*

To understand which major transmembrane HSPGs were responsible for displaying HS chains on the DC cell surface, we performed qPCR of major HS proteoglycan core proteins with and without LPS stimulation (Figure 3*A*). These included the four known syndecan core proteins expressed in mice (and humans). We identified syndecan-3 and syndecan-4 as the proteins with the highest mRNA expression in BMDCs, although syndecan-4 was dominantly expressed upon LPS stimulation. In subsequent maturation studies of nonstimulated as well as LPS-stimulated BMDCs derived from *Sdc4* knockout (*Sdc4*$^{-/-}$) mice, isolates from the mutants showed a significantly higher proportion of mature CD11c$^+$MHC-II$^+$ CD86$^+$ cells. (The majority [>98%] of BMDCs that made up the MHC-II$^+$ CD86$^+$ subset also coexpressed CCR7; data not shown.) The relative increase in mature MHC-II$^+$ CD86$^+$ BMDCs from *Sdc4*$^{-/-}$ mice compared with that of control mice with and without LPS stimulation was 29.2 ± 10.1% and 22.3 ± 10.6%, respectively (Figure 3*B*).

Ovalbumin Uptake in DCs with Altered HS

During the process of DC growth and maturation, nonspecific sampling of the local microenvironment takes place in immature DCs, whereas mature DCs demonstrate significantly reduced nonspecific endocytosis of *de novo* antigens in the immediate microenvironment. We examined the effect of altering HS N-sulfation or expression of the major HSPG core protein syndecan-4 on endocytosis using ovalbumin uptake. Ovalbumin (Ova) uptake was quantified, taking into consideration nonspecific binding

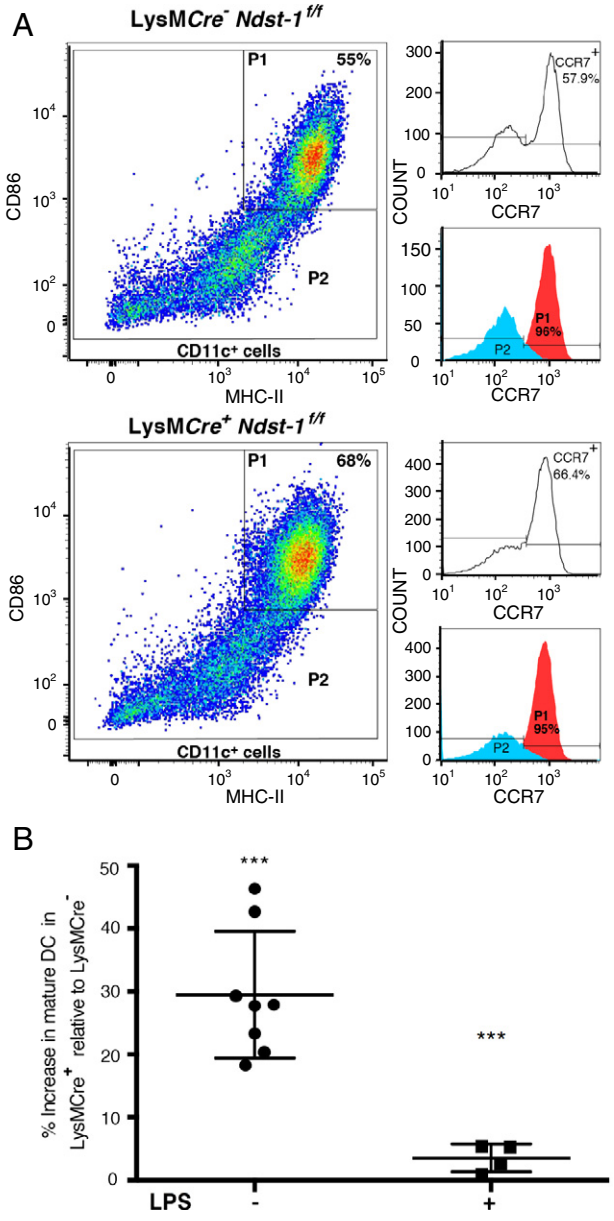

Figure 2. *Ndst1* mutation results in increased DC maturation. (A) Flow cytometry of BMDCs using maturation markers CD86, MHC-II, and CCR7: Representative panels show maturation-marker profiles for unstimulated CD11c+ BMDCs bearing the *Ndst1* mutation in HS chain sulfation (LysM*Cre* + *Ndst1f/f*) versus that of wild-type (LysM*Cre* − *Ndst-1f/f*) cells (left panels), wherein mutant cells are notable for a greater percentage of cells in the double-positive MHC-II + CD86 + subset compared with that of wild-type control BMDCs. Overall for both mutant and wild-type cells, the majority (>95%) of MHC-II + CD86 + double-positive cells were also positive for CCR7 (P1; right-side representative panels). (B) Relative % increase in mature (MHC-II + CD86 +) subset of CD11c + BMDCs isolated from LysM*Cre* + *Ndst-1f/f* mice compared with that of LysM*Cre* − *Ndst-1f/f* mice, with scatter plots for > 3 independent experiments carried out in the absence (left scatter plot) or presence (right scatter plot) of LPS. Wilcoxon signed ranked test was used for statistical analysis with a theoretical median of 0. Mean increase in maturation without LPS: 29.5 ± 10.1% and with LPS: 3.5 ± 2.2% (***$P < .0001$).

(Figure 4, representative flow cytometry histogram at top). Ova uptake was lower in *Ndst1*$^{f/f}$ *LysMCre*$^+$ mutant BMDCs relative to that of *Cre*$^-$ controls, with similar findings in *Sdc4*$^{-/-}$ BMDCs as

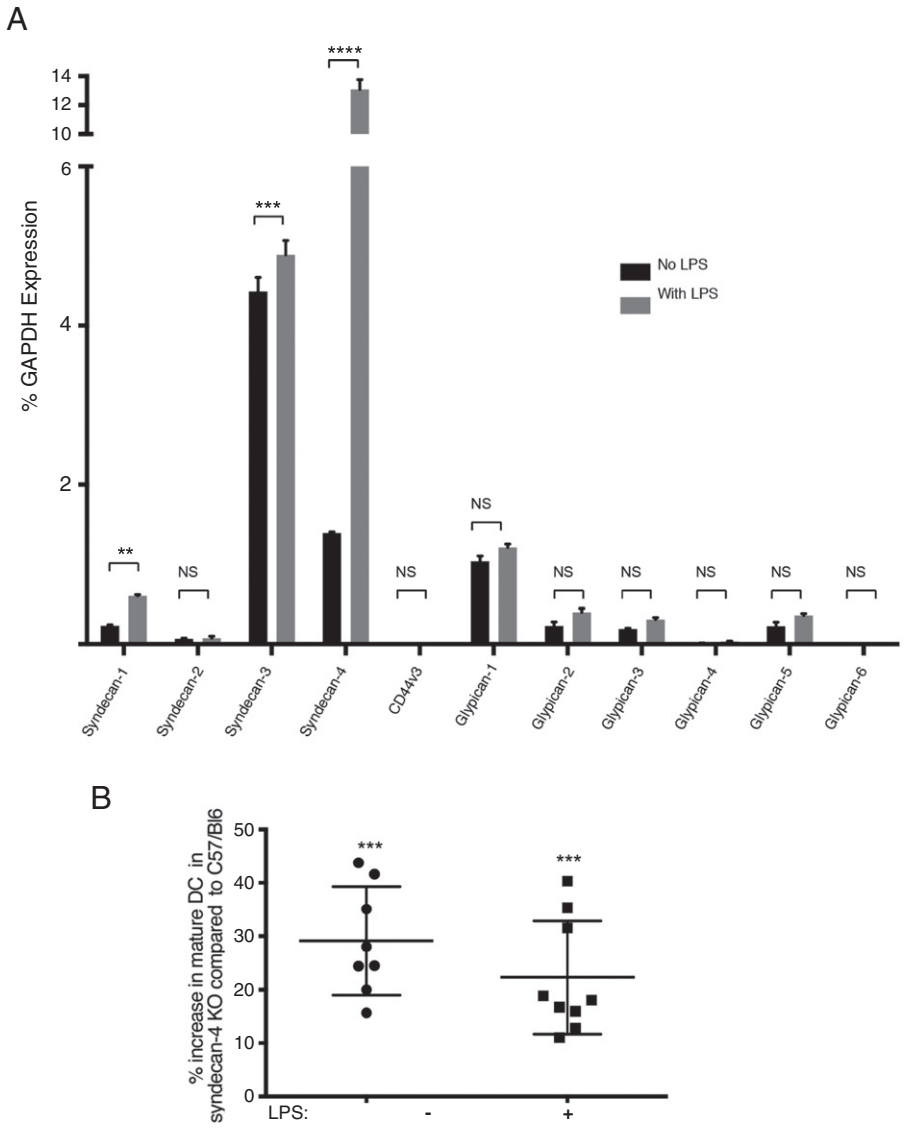

Figure 3. A mutation in the core protein for the HSPG syndecan-4 results in increased DC maturation. (A) Expression of HS proteoglycans in culture day-8 unstimulated and LPS-stimulated BMDCs from C57Bl/6 mice. Syndecan-3 and -4 and glypican-1 were highly expressed on both LPS-stimulated and unstimulated DCs. Expression was also greater in LPS-stimulated compared with unstimulated DCs, with a dominant increase in syndecan-4 expression upon LPS stimulation. Syndecan-2, glypican-1 to -6, and CD44v3 expression was unchanged before and after LPS stimulation (**$P < .01$, *** < .001; **** < .0001; NS = nonsignificant). (B) The relative percentage increase in the mature (MHC-II + CD86 +) subset of CD11c + BMDCs isolated from *Sdc4*(−/−) mutant mice compared with that of wild-type control mice, with scatter plots for multiple independent experiments carried out in the absence (left scatter plot) or presence (right scatter plot) of LPS. Wilcoxon signed ranked test was used for statistical analysis with a theoretical median of 0. Mean increase in maturation without LPS: 29.2 ± 10.1% and with LPS: 22.3 ± 10.6% (***$P < .001$).

compared with wild-type control cells. Similar findings were noted with and without LPS stimulation (see inset graphs in Figure 4, *A* and *B* showing one example of Ova uptake by *Ndst1* mutant versus control BMDCs [in *A*] and Sdc4 –/– versus control BMDCs [in *B*]). Among multiple paired BMDC isolates from mutant/wild-type mice, significant reductions in Ova uptake were demonstrated in mutants, summarized in dot plots in Figure 4*A* (for *Ndst1*-deficient cells) and Figure 4*B* (for *Sdc4*-deficient cells). The relative reduction in Ova uptake was more pronounced in immature compared with LPS-stimulated BMDCs: 41.7 ± 16.6% versus 18.6 ± 12% reduction, respectively, for *Ndst1*-deficient cells (Figure 4*A*) and 33.53 ± 7.34% versus 17.82 ± 5.87% reduction, respectively, for *Sdc4*-deficient cells (Figure 4*B*). Collectively, these findings are consistent with a more mature phenotype in BMDCs with reduced HS chain sulfation or genetic reduction in a major scaffolding core protein for HS on the BMDC cell surface.

Tumor Growth and Tumor-DC Phenotype in Mice with DCs Bearing Reduced HS Chain Sulfation

We examined whether the growth of LLC tumors might be altered in *Ndst1*$^{f/f}$ *LysMCre*$^{+}$ mutant mice given the unique myeloid alteration in HS sulfation on marrow DCs in the mutants. Tumors on the mutant background were significantly reduced in size (Figure 5*A*). Because TIDCs might also be affected by the *Ndst1*

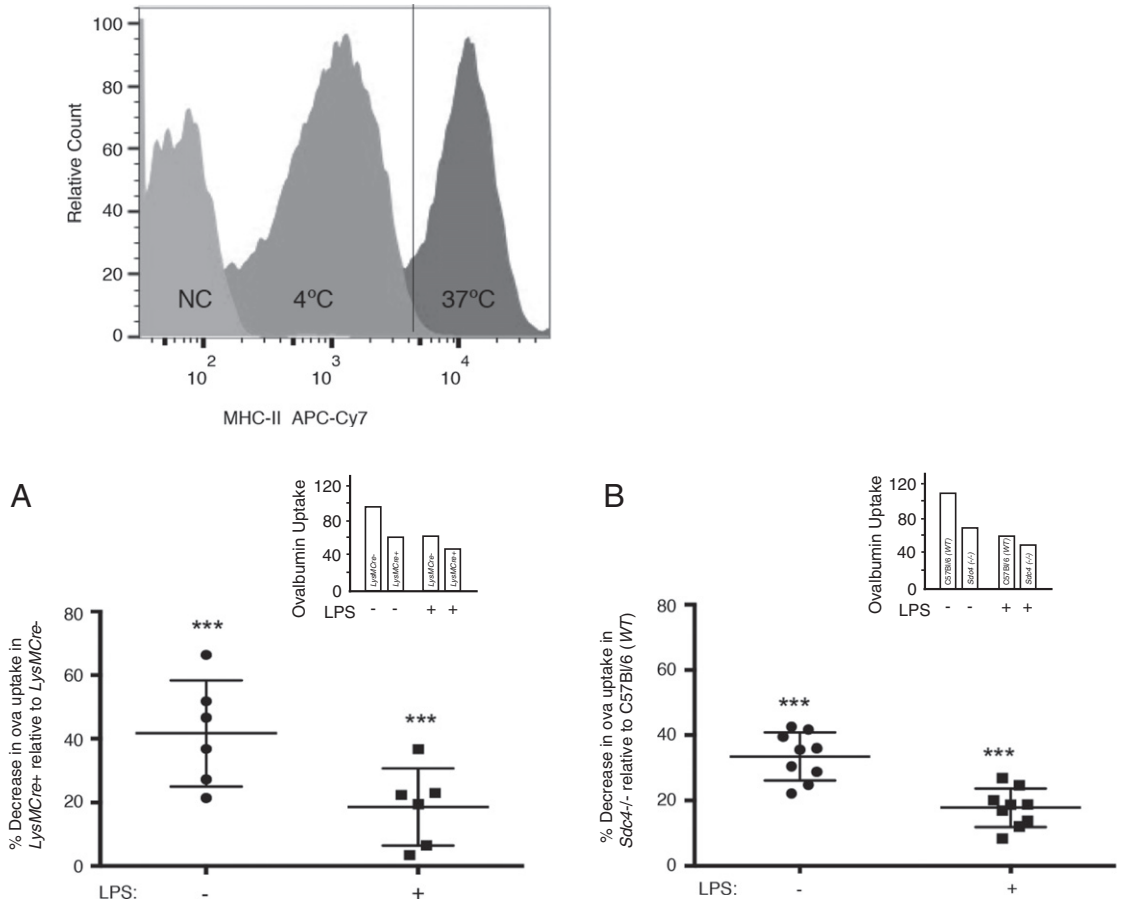

Figure 4. Dendritic cells with reduced HS chain sulfation or deficiency in the major HSPG *syndecan-4* demonstrate reduced ovalbumin uptake. Top illustration: Representative histogram of flow cytometric fluorescence-tagged Ova measurements used to quantify Ova endocytosis for DCs at 37°C. Uptake was calculated using median fluorescence intensity (MFI) at 37°C minus MFI at 4°C (nonspecific cell surface–associated Ova), divided by MFI of negative-control cells. Ova uptake = [MFI (37°C) – MFI (4°C)]/MFI (NC). (A) Scatter plot showing summary of percentage decrease in ovalbumin uptake in mutant BMDCs relative to that of control cells for multiple isolations in the absence (left) or presence (right) of LPS. Mean percentage decrease in Ova uptake without LPS: 41.7 ± 16.6% and with LPS: 18.6 ± 12%. Each data point represents an independent experiment. Wilcoxon signed ranked test was used for statistical analysis with a theoretical median of 0. (***$P < .001$.) Inset bar graph to right shows Ova uptake in a representative experiment: LysM*Cre* + *Ndst1f/f* mutant BMDCs show reduced Ova uptake compared with LysM*Cre* − *Ndst1f/f* cells in the absence (left bars) or presence (right bars) of LPS. (B) Scatter plot showing summary of percentage decrease in Ova uptake in *Sdc4* −/− BMDCs relative to that of control cells for multiple isolations in the absence (left) or presence (right) of LPS. Mean percentage decrease in Ova uptake without LPS: 33.53 ± 7.34% and with LPS: 17.82 ± 5.87%. Each data point represents an independent experiment. Wilcoxon signed ranked test was used for statistical analysis with a theoretical median of 0 (*** $P < .001$). Inset bar graph to right shows Ova uptake in a representative experiment: *Sdc4* −/− BMDCs have reduced Ova uptake compared with wild-type (C57/Bl6 background) cells with and without LPS.

mutation, we also carried out functional studies on CD11c bead-selected cells from the respective tumors, which are enriched in TIDCs. Using a transwell system similar to that used in Figure 1*A*, we found that the TIDC-enriched population from tumors in mutant mice showed reduced migration toward cultured mLECs (Figure 5*B*) and greater maturation as evidenced by MHC-II^{+} CD86^{+} expression in comparison to that of wild-type littermates (Figure 5, *C* and *D*). That population also demonstrated reduced Ova uptake (Figure 5*E*). These differences in phenotype among the CD11c+ (TIDC-enriched) populations from tumors paralleled those of BMDCs isolated in prior studies from animals with DCs harboring the same deficiency in *Ndst1*. The findings highlight the importance of how alterations in DC HS biosynthesis might translate to immunity in the pathologic state of neoplasia, with preservation of a unique DC phenotype.

Carcinoma Growth Suppression in the Setting of Systemic Syndecan-4 Deficiency, and Associated Antitumor Immunologic Profile

Knowing that a DC-targeted mutation in HS (*Ndst1* mutation) resulted in tumors with a reduced volume as well as a unique functional profile of TIDCs (Figure 5), we sought to examine tumor growth and immunity in a setting whereby the major HSPG core protein on DCs (syndecan-4; Figure 3*A*) is targeted systemically. We assessed initially how tumor growth occurs in LLC tumors on *Sdc4* –/– mutant versus wild-type backgrounds and measured tumor volumes longitudinally in the two genotypes following a subcutaneous inoculum of LLC tumor cells. Mutation was associted with a slowing in tumor growth (Figure 6*A*). Separate studies were carried out to examine tumor immunophenotype through immunologic cell harvests and flow cytometric analyses: In

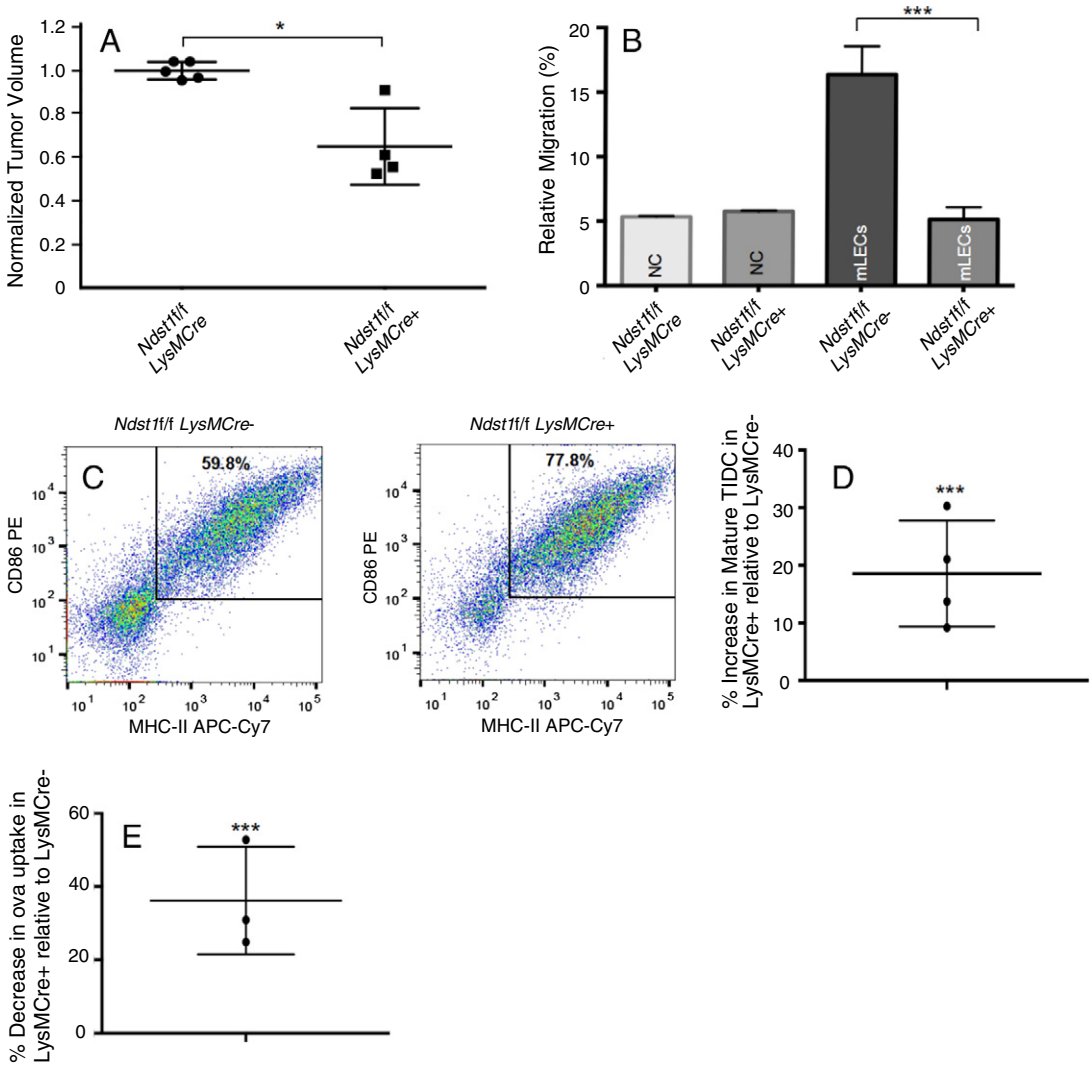

Figure 5. Mice with a DC deficiency in *Ndst1* demonstrate reduced tumor growth, along with TIDCs that are endowed with a slowed-migration/increased-maturation phenotype. (A) *Ndst1f/f* LysM*Cre* + mutant mice showed reduced growth of hindquarter-implanted LLC tumors compared with that of *Ndst1f/f* LysM*Cre* − littermate controls. This experiment is representative of two significant independent experiments. (Two-tailed unpaired *t* test was used for comparison of mean values, with comparable results and statistical significance achieved, using $P < .05$ as criterion.) (B) To assess the behavior of TIDCs harvested directly from tumors on the *Ndst1f/f* LysM*Cre* + mutant versus those from *Cre* − controls, migration assays in modified transwell systems were performed, wherein TIDCs migrated toward primary mouse lymphatic endothelial monolayers in lower wells, with altered migration of mutant TIDCs compared with that of controls (graph). This is representative of two significant independent experiments, with two-tailed unpaired *t* test used for statistical analysis (NC = negative control, wherein lower well contained no lymphatic endothelial cells). (C) Representative flow cytometry dot plot using maturation markers CD86 and MHC-II: TIDCs from *Ndst1f/f* LysM*Cre* + mutant tumor demonstrates a greater percentage of mature-subset (CD86 + MHC-II +) cells compared with *Cre* − littermate TIDCs. (D) Relative percentage increase in mature (MHC-II + CD86 +) TIDCs isolated from tumors in *Ndst1f/f* LysM*Cre* + mutant mice compared with that of *Cre* − controls in multiple experiments (represented by individual dots). Mean increase = 18.6 ± 9.2%. Wilcoxon signed ranked test was used for statistical analysis with a theoretical median of 0. (E) Scatter plot representing the average percentage decrease of ovalbumin uptake of TIDCs isolated from tumors in *Ndst-1f/f* LysM*Cre* + mice compared with that of *Cre* − controls in multiple experiments (represented by individual dots). Mean decrease = 36.2 ± 14.6%. Wilcoxon signed ranked test was used for statistical analysis with a theoretical median of 0. (*$P < .05$; **$P < .01$; ***$P < .001$.)

an independent tumor set, with tumor size again significantly reduced in *Sdc4*−/− mutant mice at time of cell harvest (Figure 6*B*, *left*), tumors on the mutant background showed an increase in the relative degree of infiltration by mature CD11c+ cells, which include the TIDC subset (Figure 6*B*, *right* and *C with graph*). In addition, tumors on the *Sdc4*−/− background were noted to have significantly higher degrees of infiltration by NK cells and NKT cells (Figure 6*D*, *left* and *middle graphs*), which typically consitute important effector immune cells during robust antitumor responses [35]. There was also an increase in infiltration by the $Nk1.1^{-}$ $Thy1.2/CD19^{+}$ subpopulation in tumors on the *Sdc4*−/− background (refer to gating strategy in Figure 6*B*), which indicated that tumor overall infiltration by T/B cells is increased in the mutants (Figure 6*D*, *right*).

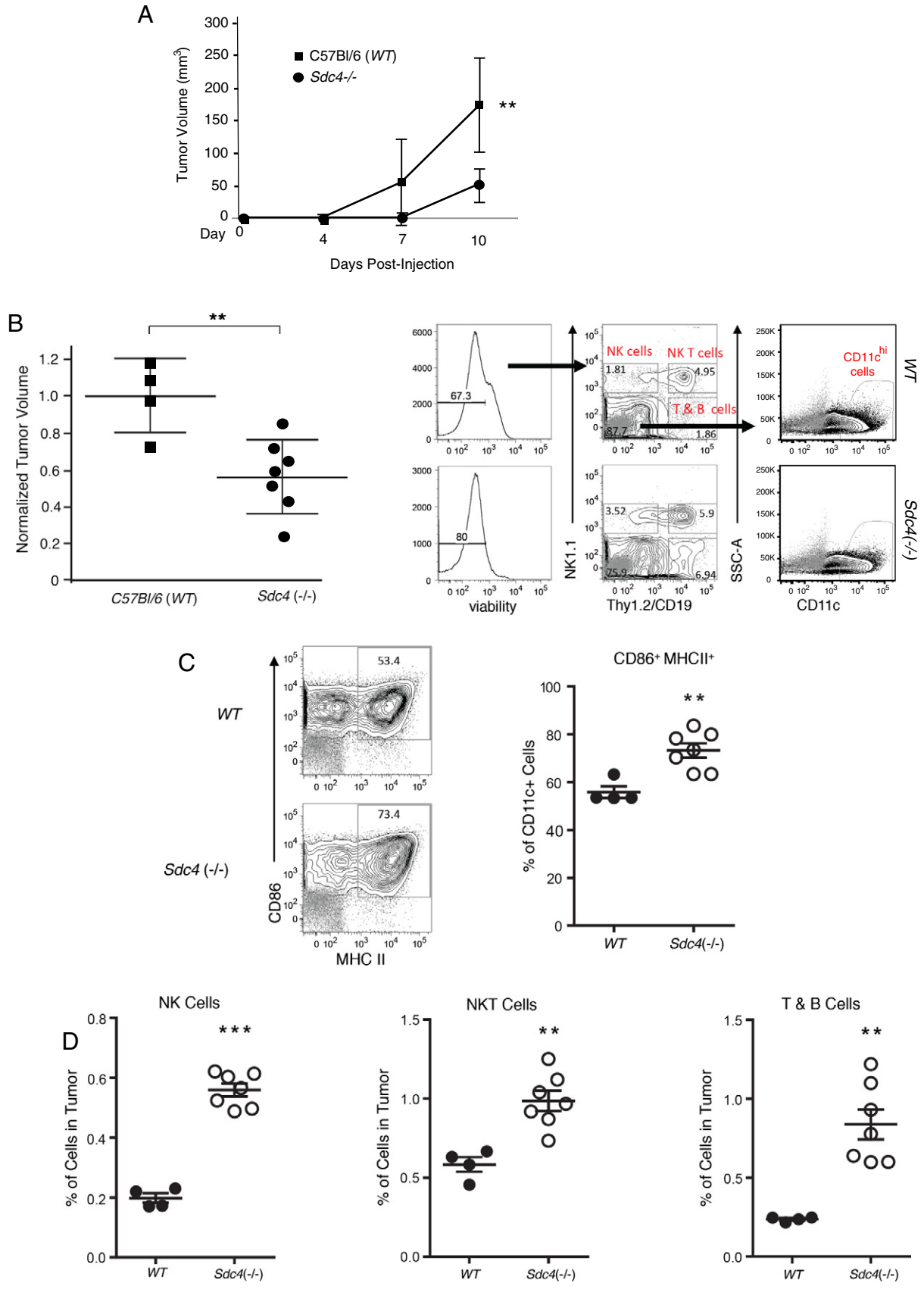

Discussion

In the lymphatic microenvironment, HS has been found to play important roles in the formation of chemokine gradients as well as the recruitment of inflammatory and immune cells into lymphatic vessels [36]. Whether and how the glycan HS produced by DCs might possibly play a role in mediating basic DC functions have remained a

mystery. Findings herein support an important role for this glycan in mediating both chemokine-driven DC trafficking as well as maturation *in vitro* and *in vivo*, a unique phenotype that is preserved in both BMDCs and TIDCs.

The reduced lymphatic endothelium-directed trafficking of *Ndst1*-deficient DCs is noted in both immature as well as mature DCs and is not caused by a reduction in expression of the chemokine receptor CCR7 or in the maturation markers CD86 and MHCII (Figure 2). On the contrary, these markers are significantly increased along with reduced ovalbumin uptake, consistent with a more mature phenotype. CCL21 is a major chemokine responsible for DC migration from peripheral tissues toward lymph nodes [37]. Cell-bound CCL21, a chemokine that binds strongly to HS, facilitates adhesion and random migration of DCs. This is distinguished from CCL19, a chemokine that does not bind to HS, and causes migration directed toward the source of the soluble chemokine without a significant role in adhesion of DCs [38,39]. Interestingly, because *Ndst1*-deficient DCs showed reduced migration toward both CCL21 and CCL19 (Supplemental Figure S2), mechanistic importance may also lie in the ability of the glycan to mediate receptor (i.e., CCR7) activity. This implies a possible key role for the glycan chain as part of a proteoglycan co-receptor. This is also consistent with our discovery of syndecan-4 as a putative co-receptor. Regardless, with respect to HS-binding ligands such as CCL21 (or others in the lymphatic microenvironment), interactions of basic amino acid–rich domains of a given chemokine with the sulfated glycan may critically regulate cell surface availability, concentrations, and gradients of the chemokine.

The phenotype we have encountered as a result of generating DCs with a sulfate-modifying mutation in the glycan (or genetic absence of the major core protein syndecan-4) *in vivo* is characterized by a reduction in migration potential in association with an increase in maturation. Although these may be independently related to the mutation, they are also linked in the setting of DC function following activation with unique stimuli. The effect of mutation on reducing early Akt phosphorylation following CCL21 stimulation may be sufficient to inhibit migration signaling by CCL21-responsive DCs. This is in a setting in which the altered glycan chain in mutants can impair the ability of the glycan to serve as a co-receptor for GPCR signaling. Following exposure to a maturation signal such as a bacterial endotoxin, DC antigen uptake is typically shut down after a transient increase [40–42]. This is followed by an upregulation of CCR7 and a concomitant increase in CCL19- and CCL21-driven traffic [43–45]. This allows DCs to shift from immature cells proficient in antigen uptake to mature lymph node migratory cells that are relatively more efficient in MHC restricted antigen presentation and the priming of naive T cells [42,46]. It should be recognized, however, that maturation and migration are not always coupled and may be induced in DCs relatively independently in some settings. In one study, human monocyte-derived DCs showed increased migration upon exposure to soluble glycan, without necessarily the equivalent change in maturation [47]. Also, BMDCs deficient in heparinase or transfected with CCR7 receptor showed reduced and increased migration, respectively, with minimal or no change in maturation [48,49].

A few mechanisms might explain the DC phenotype induced by an alteration in the sulfation of HS or the absence of a major proteoglycan that tethers the glycan to the DC surface. Firstly, a simple alteration in the anionic state of sulfated domains on HS chains may be essential for disrupting the binding to multiple chemokines or for altering the chemokine ligand-receptor interaction [4]. Secondly, it has been previously demonstrated that loss of cell surface HS chains may be associated with either increased shedding of syndecan-1 and/or syndecan-4 (as demonstrated in multiple human and mouse cell lines) or a marked increase in core protein synthesis. The increased shedding could be secondary to an enhanced proteolytic cleavage of the HSPG core protein by matrix metalloproteinases [50,51]. Curiously, increased shedding could also lead to changes in the DC microenvironment that may indirectly alter DC maturation, as soluble proteoglycans have been shown to induce maturation of DCs by acting as direct TLR4 agonists [14–16].

We observed syndecan-4 to be a dominant HSPG on DCs, especially upon stimulation with LPS (Figure 3*A*). Human monocyte-derived DCs express a complex array of syndecans and glypicans that change with their degree of maturation [52]. Increased maturation of human monocyte-derived DCs (including Langerhans cells) has been noted to occur with a shift from dominant syndecan-1 expression to that of syndecan-4 [25]. In our expression studies, syndecan-4 along with syndecan-1 (to a lesser degree) was significantly increased in association with exposure to maturation stimuli, including LPS (Figure 3*A*) as well as TNFα (Supplemental Figure S4). Interestingly, when we looked specifically at DCs deficient in syndecan-4, we also noted a significant increase in maturation markers MHCII, CD86, and CCR7 along with a decrease in antigen uptake. These findings emphasize that both HS and major HS core proteins on DCs play important roles in the regulation of DC maturation (Figures 2 and 3). Intriguingly, a recent report examines the effect of genetic deficiency in syndecan-4 on reduced pathologic DC migration associated with an asthma model [24]. This is consistent with our findings of slowed lymphatic-directed DC trafficking with a DC-directed mutation in the HS chain itself (Figures 1, *A* and B, and 5*B*). In our studies following discovery that *Sdc4* was strongly expressed (especially upon LPS stimulation) in marrow-derived DCs, we found relative hypermaturation in DCs

Figure 6. Reduced tumor growth and antitumor immune phenotype in syndecan-4–deficient mice. (A) Lewis lung carcinomas were implanted subcutaneously in the hindquarter of *Sdc4*−/− mice (backcrossed onto C57Bl/6 background) and wild-type (*WT*) C57Bl/6 controls. We assessed initially how tumor growth occurs longitudinally in the two genotypes, with graph showing comparison of growth curves. (B) In a separate tumor growth for immunophenotyping (confirming again a reduction in the mean tumor volume in *Sdc4* mutants normalized to that of wild-type littermates at time of cell harvest; dot plot at left), whole-cell digests from tumors were analyzed by flow cytometry. The data are representative of two independent experiments (with two-tailed unpaired *t* test used to compare means, and statistical significance achieved in independent experiments). At right, initial gating strategies are shown for viable cells, lineages, and selection of CD11c(hi) subsets (NK cells: $Nk1.1^{+}Thy1.2/CD19^{-}$; NKT cells: $NK1.1^{+}Thy1.2/CD19^{+}$; T&B cells: $Nk1.1^{-}Thy1.2/CD19^{+}$; $CD11c^{hi}$ cells: Nk1.1-Thy1.2/CD19-CD11c(hi)). Representative FACS plots are shown for *WT* and *Sdc4*−/−. (C) Gating of MHCII and CD86 double-positive cells as a percentage of the respective CD11c(hi) subsets is shown for a representative example (left), and graph of proportions of double-positive cells is shown at right. (D) Proportions of NK, NKT, and T & B cells within mouse tumors are graphed. Graphs depict individual mouse tumors and mean ± SEM. **P* < .05, ***P* < .01, ****P* < .001.

isolated from the the mutants, a phenotype which may be causally associated with altered migration. In this regard, by genetically targeting sulfation of the glycan "business end" of proteoglycans on DCs (i.e., moiety that directly interacts with chemokines and/or receptor ternary complexes), the result is both slowed lymphatic-directed DC migration as well as increased DC maturation. It is possible that exposure of classic DCs to maturation stimuli, including some that are expressed in tumor microenvironment, is associated with a regulatory rise in *Sdc4* expression (Figure 3*A* and Supplemental Figure S4) as a secondary or homeostatic response. Regardless, genetic ablation in *Sdc4* expression appears to be sufficient to promote maturation independent of a key DC-maturation ligand such as LPS (Figure 3*B*). Moreover, our findings also point to the likelihood that the DC phenotype resulting from such glycan targeting may inhibit pathologic immunosuppressive effects of tolerogenic-DC migration and immaturity on tumor growth (Figure 5).

In tumor microenvironment, DCs may play roles in priming T cells and in tumor rejection; however, tumor-associated DCs are often deregulated and polarized into a tolerogenic state, allowing tumor cells to escape immune surveillance [53]. Because reduction in the sulfation of HS leads to a more mature DC phenotype, along with lower lymph node directed motility, we examined whether the phenotypes might affect tumor growth. The latter may be altered by greater antitumor immunity that might exist in a state of increased DC maturation and reduced traffic of tolerogenic DCs to the draining lymph nodes. Indeed, mice genetically deficient in *Ndst1* in the myeloid compartment harbored smaller experimental LLC tumors than that of wild-type littermates. Importantly, the CD11c+ fraction from tumors in mutant mice showed reduced migration toward lymphatic endothelium as well as a more mature phenotype (Figure 5). This is consistent with a more mature phenotype of DCs in the setting of cancer and thus may represent an attractive immunophenotype.

We extended our carcinoma model analyses to *Sdc4* mutant mice given findings from HSPG expression data (Figure 3*A* and Supplemental Figure S4). Given that syndecan-4 might serve as a key co-receptor that harbors a substantial amount of the HS (i.e., genetically targeted in TIDCs in Figure 5), we examined tumor growth in *Sdc4*−/− mutants. Growth was inhibited on this background (Figure 6*A*), and we carried out further immunophenotyping studies, confirming again that tumors were not only smaller on the *Sdc4* −/− background but more heavily endowed with mature TIDCs in the mutant mice. Moreover, the greater infiltration by NK and NKT cells in mutants implies the induction of a profile of cell-mediated antitumor immunity as a result of mutation [35]. A potential clinical-translation consideration is that our examination of tumor growth and antitumor immunity in *Sdc4* systemic-mutant/knockout mice also may also be analagous to how antitumor immunity might be enhanced during treatment with an inhibitor of syndecan-4. In that setting, reduction in HS expression on DCs may be achieved while sparing HS chains in other tissues where syndecan-4 does not dominate.

Although a limitation of this work is that the *LysM* transgene is also expressed in myeloid-derived cells in addition to DCs (such as macrophages), which could affect the observed phenotype, it is compelling to find the preserved phenotype in tumor-derived DCs (TIDCs) purified from mutant tumors. The use of this model may be considered in light of other transgenic *Cre* models that are used to target the myeloid compartment (e.g., *CD11c Cre*). The latter may also have some limitations, as CD11c is also expressed on macrophages [54] and mature mouse DCs downregulate their expression of CD11c [55].

Conclusions

Targeting the sulfation of HS on DCs appears to endow such cells with reduced chemokine-dependent motility and increased maturation. Although the importance of cell-surface glycans in GPCR signaling by DCs may provide some mechanistic insight, the qualities appear to be preserved by tumor DCs and are associated with reduced tumor growth *in vivo*. Moreover, a major proteoglycan, syndecan-4, appears to be a dominant scaffold for HS chains on the DC surface, and targeting this proteoglycan (as a key tumor-chemokine co-receptor) also results in reduced tumor growth with a favorable tumor immunologic profile. These findings provide rationale for targeting DC HS and even syndecan-4 as a novel approach to improve antitumor immunity in cancer.

Acknowledgements

We appreciate advice and assistance from Jeffrey Esko, including assistance with *Ndst1*$^{f/f}$ *LysMCre*$^{+}$ mutants, and we acknowledge Paul Goetinck for *Sdc4* homozygous-null mice. We thank Paul Clopton of the VA San Diego Healthcare System for statistical assistance and Faye Nourollahi for assistance with some unique culture and genotyping procedures as well as PCR studies.

Appendix A. Supplementary data

Supplementary data to this article can be found online at http://dx.doi.org/10.1016/j.neo.2016.04.004.

References

[1] Steinman RM, Hawiger D, and Nussenzweig MC (2003). Tolerogenic dendritic cells. *Annu Rev Immunol* **21**, 685–711.
[2] Wallet MA, Sen P, and Tisch R (2005). Immunoregulation of dendritic cells. *Clin Med Res* **3**(3), 166–175.
[3] Schmidt SV, Nino-Castro AC, and Schultze JL (2012). Regulatory dendritic cells: there is more than just immune activation. *Front Immunol* **3**, 274.
[4] Bishop JR, Schuksz M, and Esko JD (2007). Heparan sulphate proteoglycans fine-tune mammalian physiology. *Nature* **446**(7139), 1030–1037.
[5] Kjellen L, Pettersson I, and Höök M (1981). Cell-surface heparan sulfate: an intercalated membrane proteoglycan. *Proc Natl Acad Sci U S A* **78**(9), 5371–5375.
[6] Kanwar YS and Farquhar MG (1979). Isolation of glycosaminoglycans (heparan sulfate) from glomerular basement membranes. *Proc Natl Acad Sci U S A* **76**(9), 4493–4497.
[7] Hedman K, Johansson S, Vartio T, Kjellén L, Vaheri A, and Höök M (1982). Structure of the pericellular matrix: association of heparan and chondroitin sulfates with fibronectin-procollagen fibers. *Cell* **28**(3), 663–671.
[8] Key NS, Platt JL, and Vercellotti GM (1992). Vascular endothelial cell proteoglycans are susceptible to cleavage by neutrophils. *Arterioscler Thromb* **12**(7), 836–842.
[9] Geller RL, Ihrcke NS, Maines J, Lindman BJ, and Platt JL (1993). Loss of heparan sulfate proteoglycan as a manifestation of cellular immunity in vivo and *in vitro*. *Transplant Proc* **25**(1 Pt 1), 144–145.
[10] Ihrcke NS, Wrenshall LE, Lindman BJ, and Platt JL (1993). Role of heparan sulfate in immune system-blood vessel interactions. *Immunol Today* **14**(10), 500–505.
[11] Johnson GB, Brunn GJ, Kodaira Y, and Platt JL (2002). Receptor-mediated monitoring of tissue well-being via detection of soluble heparan sulfate by Toll-like receptor 4. *J Immunol* **168**(10), 5233–5239.
[12] Wrenshall LE, Cerra FB, Carlson A, Bach FH, and Platt JL (1991). Regulation of murine splenocyte responses by heparan sulfate. *J Immunol* **147**(2), 455–459.
[13] Bruserud O and Lundin K (1987). The effect of drugs used in anticoagulation therapy on T lymphocyte activation *in vitro*. II. Warfarin inhibits T lymphocyte activation. *J Clin Lab Immunol* **23**(4), 169–173.

[14] Kodaira Y, Nair SK, Wrenshall LE, Gilboa E, and Platt JL (2000). Phenotypic and functional maturation of dendritic cells mediated by heparan sulfate. *J Immunol* **165**(3), 1599–1604.

[15] Brennan TV, Lin L, Huang X, Cardona DM, Li Z, Dredge K, Chao NJ, and Yang Y (2012). Heparan sulfate, an endogenous TLR4 agonist, promotes acute GVHD after allogeneic stem cell transplantation. *Blood* **120**(14), 2899–2908.

[16] Wrenshall LE, Stevens RB, Cerra FB, and Platt JL (1999). Modulation of macrophage and B cell function by glycosaminoglycans. *J Leukoc Biol* **66**(3), 391–400.

[17] Xia CQ and Kao KJ (2002). Heparin induces differentiation of CD1a+ dendritic cells from monocytes: phenotypic and functional characterization. *J Immunol* **168**(3), 1131–1138.

[18] Delirezh N, Majedi L, Asri Rezaei S, and Ranjkeshzadeh H (2011). Generation of mature monocyte-derived dendritic cells in the presence of heparin and monocyte conditioned medium: phenotypic and functional comparison. *Iran Biomed J* **15**(3), 79–84.

[19] Lortat-Jacob H, Grosdidier A, and Imberty A (2002). Structural diversity of heparan sulfate binding domains in chemokines. *Proc Natl Acad Sci U S A* **99**(3), 1229–1234.

[20] Lau EK, Allen S, Hsu AR, and Handel TM (2004). Chemokine-receptor interactions: GPCRs, glycosaminoglycans and viral chemokine binding proteins. *Adv Protein Chem* **68**, 351–391.

[21] Wang L, Fuster M, Sriramarao P, and Esko JD (2005). Endothelial heparan sulfate deficiency impairs L-selectin– and chemokine-mediated neutrophil trafficking during inflammatory responses. *Nat Immunol* **6**(9), 902–910.

[22] Middleton J, Neil S, Wintle J, Clark-Lewis I, Moore H, Lam C, Auer M, Hub E, and Rot A (1997). Transcytosis and surface presentation of IL-8 by venular endothelial cells. *Cell* **91**(3), 385–395.

[23] Lander AD, Nie Q, and Wan FY (2002). Do morphogen gradients arise by diffusion? *Dev Cell* **2**(6), 785–796.

[24] Polte T, Petzold S, Bertrand J, Schütze N, Hinz D, Simon JC, Lehmann I, Echtermeyer F, Pap T, and Averbeck M (2015). Critical role for syndecan-4 in dendritic cell migration during development of allergic airway inflammation. *Nat Commun* **6**, 7554.

[25] Averbeck M, Gebhardt C, Anderegg U, Termeer C, Sleeman JP, and Simon JC (2007). Switch in syndecan-1 and syndecan-4 expression controls maturation associated dendritic cell motility. *Exp Dermatol* **16**(7), 580–589.

[26] Bühligen J, Himmel M, Gebhardt C, Simon JC, Ziegler W, and Averbeck M (2010). Lysophosphatidylcholine-mediated functional inactivation of syndecan-4 results in decreased adhesion and motility of dendritic cells. *J Cell Physiol* **225**(3), 905–914.

[27] Inaba K, Swiggard WJ, Steinman RM, Romani N, Schuler G, and Brinster C (2009). Isolation of dendritic cells. *Curr Protoc Immunol* , 7 [Chapter 3: Unit 3].

[28] Lin C, Ear J, Midde K, Lopez-Sanchez I, Aznar N, Garcia-Marcos M, Kufareva I, Abagyan R, and Ghosh P (2014). Structural basis for activation of trimeric Gi proteins by multiple growth factor receptors via GIV/Girdin. *Mol Biol Cell* **25**(22), 3654–3671.

[29] Livak KJ and Schmittgen TD (2001). Analysis of relative gene expression data using real-time quantitative PCR and the 2(– Delta Delta C(T)) method. *Methods* **25**(4), 402–408.

[30] Weber M, Hauschild R, Schwarz J, Moussion C, de Vries I, Legler DF, Luther SA, Bollenbach T, and Sixt M (2013). Interstitial dendritic cell guidance by haptotactic chemokine gradients. *Science* **339**(6117), 328–332.

[31] Yin X, Truty J, Lawrence R, Johns SC, Srinivasan RS, Handel TM, and Fuster MM (2010). A critical role for lymphatic endothelial heparan sulfate in lymph node metastasis. *Mol Cancer* **9**, 316.

[32] Lindahl U and Kjellen L (2013). Pathophysiology of heparan sulphate: many diseases, few drugs. *J Intern Med* **273**(6), 555–571.

[33] Ruse M and Knaus UG (2006). New players in TLR-mediated innate immunity: PI3K and small Rho GTPases. *Immunol Res* **34**(1), 33–48.

[34] Agrawal A, Agrawal S, Cao JN, Su H, Osann K, and Gupta S (2007). Altered innate immune functioning of dendritic cells in elderly humans: a role of phosphoinositide 3-kinase-signaling pathway. *J Immunol* **178**(11), 6912–6922.

[35] Swann JB and Smyth MJ (2007). Immune surveillance of tumors. *J Clin Invest* **117**(5), 1137–1146.

[36] Bao X, Moseman EA, Saito H, Petryniak B, Thiriot A, Hatakeyama S, Ito Y, Kawashima H, Yamaguchi Y, Lowe JB, von Andrian UH, and Fukuda M (2010). Endothelial heparan sulfate controls chemokine presentation in recruitment of lymphocytes and dendritic cells to lymph nodes. *Immunity* **33**(5), 817–829.

[37] Bajénoff M, Egen JG, Koo LY, Laugier JP, Brau F, Glaichenhaus N, and Germain RN (2006). Stromal cell networks regulate lymphocyte entry, migration, and territoriality in lymph nodes. *Immunity* **25**(6), 989–1001.

[38] Schumann K, Lämmermann T, Bruckner M, Legler DF, Polleux J, Spatz JP, Schuler G, Förster R, Lutz MB, Sorokin L, and Sixt M (2010). Immobilized chemokine fields and soluble chemokine gradients cooperatively shape migration patterns of dendritic cells. *Immunity* **32**(5), 703–713.

[39] de Paz JL, Moseman EA, Noti C, Polito L, von Andrian UH, and Seeberger PH (2007). Profiling heparin-chemokine interactions using synthetic tools. *ACS Chem Biol* **2**(11), 735–744.

[40] Sallusto F, Cella M, Danieli C, and Lanzavecchia A (1995). Dendritic cells use macropinocytosis and the mannose receptor to concentrate macromolecules in the major histocompatibility complex class II compartment: downregulation by cytokines and bacterial products. *J Exp Med* **182**(2), 389–400.

[41] Sallusto F and Lanzavecchia A (1994). Efficient presentation of soluble antigen by cultured human dendritic cells is maintained by granulocyte/macrophage colony-stimulating factor plus interleukin 4 and downregulated by tumor necrosis factor alpha. *J Exp Med* **179**(4), 1109–1118.

[42] Granucci F, Ferrero E, Foti M, Aggujaro D, Vettoretto K, and Ricciardi-Castagnoli P (1999). Early events in dendritic cell maturation induced by LPS. *Microbes Infect* **1**(13), 1079–1084.

[43] Dieu MC, Vanbervliet B, Vicari A, Bridon JM, Oldham E, Aït-Yahia S, Brière F, Zlotnik A, Lebecque S, and Caux C (1998). Selective recruitment of immature and mature dendritic cells by distinct chemokines expressed in different anatomic sites. *J Exp Med* **188**(2), 373–386.

[44] Sallusto F, Schaerli P, Loetscher P, Schaniel C, Lenig D, Mackay CR, Qin S, and Lanzavecchia A (1998). Rapid and coordinated switch in chemokine receptor expression during dendritic cell maturation. *Eur J Immunol* **28**(9), 2760–2769.

[45] Sozzani S, Allavena P, D'Amico G, Luini W, Bianchi G, Kataura M, Imai T, Yoshie O, Bonecchi R, and Mantovani A (1998). Differential regulation of chemokine receptors during dendritic cell maturation: a model for their trafficking properties. *J Immunol* **161**(3), 1083–1086.

[46] Alvarez D, Vollmann EH, and von Andrian UH (2008). Mechanisms and consequences of dendritic cell migration. *Immunity* **29**(3), 325–342.

[47] Yoshino H, Takahashi K, Monzen S, and Kashiwakura I (2010). Proteoglycans regulate the chemotaxis of dendritic cells derived from human peripheral blood monocytes. *Biol Pharm Bull* **33**(6), 938–944.

[48] Benhamron S, Reiner I, Zcharia E, Atallah M, Grau A, Vlodavsky I, and Mevorach D (2012). Dissociation between mature phenotype and impaired transmigration in dendritic cells from heparanase-deficient mice. *PLoS One* **7**(5)e35602.

[49] Xin HM, Peng YZ, Yuan ZQ, and Guo H (2009). *In vitro* maturation and migration of immature dendritic cells after chemokine receptor 7 transfection. *Can J Microbiol* **55**(7), 859–866.

[50] Ramani VC, Pruett PS, Thompson CA, DeLucas LD, and Sanderson RD (2012). Heparan sulfate chains of syndecan-1 regulate ectodomain shedding. *J Biol Chem* **287**(13), 9952–9961.

[51] Yang Y, Macleod V, Miao HQ, Theus A, Zhan F, Shaughnessy Jr JD, Sawyer J, Li JP, Zcharia E, Vlodavsky I, and Sanderson RD (2007). Heparanase enhances syndecan-1 shedding: a novel mechanism for stimulation of tumor growth and metastasis. *J Biol Chem* **282**(18), 13326–13333.

[52] Wegrowski Y, Milard AL, Kotlarz G, Toulmonde E, Maquart FX, and Bernard J (2006). Cell surface proteoglycan expression during maturation of human monocytes-derived dendritic cells and macrophages. *Clin Exp Immunol* **144**(3), 485–493.

[53] Ma Y, Shurin GV, Peiyuan Z, and Shurin MR (2013). Dendritic cells in the cancer microenvironment. *J Cancer* **4**(1), 36–44.

[54] Hume DA (2008). Macrophages as APC and the dendritic cell myth. *J Immunol* **181**(9), 5829–5835.

[55] Singh-Jasuja H, Thiolat A, Ribon M, Boissier MC, Bessis N, Rammensee HG, and Decker P (2013). The mouse dendritic cell marker CD11c is down-regulated upon cell activation through Toll-like receptor triggering. *Immunobiology* **218**(1), 28–39.